



HAL
open science

Importance of excitonic effects and the question of internal electric fields in stacking faults and crystal phase quantum discs: the model-case of GaN.

Pierre Corffdir, Pierre Lefebvre

► To cite this version:

Pierre Corffdir, Pierre Lefebvre. Importance of excitonic effects and the question of internal electric fields in stacking faults and crystal phase quantum discs: the model-case of GaN.. *Journal of Applied Physics*, 2012, 112 (5), pp.053512. 10.1063/1.4749789 . hal-00750406

HAL Id: hal-00750406

<https://hal.science/hal-00750406>

Submitted on 6 Jul 2023

HAL is a multi-disciplinary open access archive for the deposit and dissemination of scientific research documents, whether they are published or not. The documents may come from teaching and research institutions in France or abroad, or from public or private research centers.

L'archive ouverte pluridisciplinaire **HAL**, est destinée au dépôt et à la diffusion de documents scientifiques de niveau recherche, publiés ou non, émanant des établissements d'enseignement et de recherche français ou étrangers, des laboratoires publics ou privés.

Importance of excitonic effects and the question of internal electric fields in stacking faults and crystal phase quantum discs: the model-case of GaN

Pierre Corfdir^{1,a)}, and Pierre Lefebvre^{2,3}

¹*Cavendish Laboratory, University of Cambridge, J. J. Thomson Avenue, Cambridge CB3 0HE, United Kingdom.*

²*CNRS, Laboratoire Charles Coulomb, UMR5221, 34095 Montpellier, France.*

³*Université Montpellier 2, Laboratoire Charles Coulomb, UMR5221, 34095 Montpellier, France.*

Abstract

We compute using envelope function calculations the energy and the oscillator strength of excitons in zinc-blende / wurtzite quantum wells (QWs), such as those that appear in many examples of semiconductor nanowires, and in basal plane stacking faults (BSFs). We address specifically the model-case of GaN. In addition to the electron-hole Coulomb interaction, we account for the quantum-confined Stark effect. We demonstrate that despite the type-II band alignment, a significant binding and a rather strong oscillator strength are preserved by excitonic effects. When adjacent crystal phase QWs are coupled together, we compute increased as well as decreased exciton oscillator strength with respect to the single QW case, depending on the BSF-BSF coupling scheme. Comparing the results of our calculations with available data, we finally conclude in favor of the absence of built-in electric fields perpendicular to the BSF planes.

^{a)}Electronic mail: pmc53@cam.ac.uk

I. Introduction

In recent years, a considerable effort has been devoted to the study of semiconductor nanowires [1]. One of the unique characteristics of III-V semiconductor nanowires is the fact that they typically crystallize into a wurtzite (WZ) geometry instead of the zinc-blende (ZB) crystal structure more common in the bulk materials. However, even though WZ is the most stable crystal structure for III-V nanowires, they are usually polytypic, *i.e.* they present large densities of ZB inclusions [2,3]. In particular, WZ nanowires exhibit high densities of I₁-type basal plane stacking faults (BSFs), an extended kind of defect that can be seen as a three monolayer-thick inclusion of ZB material [3]. Despite the fact that the presence of ZB/WZ interfaces is generally considered as detrimental to carrier transport properties [4], the polytypism of III-V nanowires provides a unique route to novel confinement within nanowires. As shown by *ab initio* calculations [5], planar ZB inclusions in the WZ phase of a III-V semiconductor should behave as shallow type-II quantum wells (QWs), where electrons are confined in the ZB layers. This prediction has motivated research into finer control of the III-V nanowire growth, as the modulation of the phase along the length of a single semiconductor nanowire allows for a new kind of bandgap engineering. As a result, it is now possible to realize purely ZB [6] or WZ [7] GaAs nanowires and crystal phase tuning along the length of single InAs and InP nanowires has been demonstrated [2,3]. In the case of GaN, even though WZ nanowires grown by molecular beam epitaxy are typically defect-free [8], it is possible to induce stacking faults using catalyst-based growth conditions [9].

Despite the progress in growth and characterization of nanowires with polytypic faults, there have been, so far, only a few attempts at modeling the emission properties of crystal phase quantum disks [10-13] (we define as a crystal phase quantum disk [14] a ZB/WZ QW in a microwire, where the lateral confinement is negligible). In addition, until now excitonic effects have been systematically neglected [10-13], based on the assumption that due to the type-II band alignment between WZ and ZB phases, the binding energy of the exciton should be small compared to the bulk case [10]. However, as pointed out in Refs. 15 and 16, the electron (*hole*) wave function of an exciton confined in a ZB/WZ QW should show large penetration in the WZ (*ZB*) phase. Consequently, we show in the following that excitonic effects should be quite significant. In some cases the excitonic binding energy will actually be larger than that in the bulk, leading to drastic variations in both the emission energy and oscillator strength compared to the case of unbound electron-hole pairs.

In this paper, we compute the energy and the oscillator strength for excitons confined in (111) ZB / (0001) WZ crystal phase QWs, and specifically in the most elementary case of BSFs. In particular, we show the effect of coupling between adjacent QWs and of internal polarization discontinuities at the WZ/ZB interfaces. Although our modeling procedure can be applied to any III-V material, we address specifically the case of GaN, as there is, for this material, a general agreement between the ZB/WZ valence and conduction band offsets determined experimentally and those obtained theoretically.

II. Formalism

With the z -axis parallel to the ZB [111] and WZ [0001] directions (the confinement axis), the Schrödinger equation for an electron-hole pair in a WZ/ZB structure is:

$$\left\{ -\frac{\hbar^2}{2} \left(\frac{\partial}{\partial z_e} \left[\frac{1}{m_e} \frac{\partial}{\partial z_e} \right] + \frac{\partial}{\partial z_h} \left[\frac{1}{m_h} \frac{\partial}{\partial z_h} \right] \right) - \frac{\hbar^2}{2\mu_{\perp}} \nabla_{\rho}^2 + V_e(z_e) + V_h(z_h) - \frac{e^2}{4\pi\epsilon\sqrt{(z_e - z_h)^2 + \rho^2}} \right\} \Phi_{\text{ex}} = E_{\text{ex}} \Phi_{\text{ex}}$$

Eq. (1),

where z_e , z_h and $\rho = \rho_e - \rho_h$ are the electron and hole on-axis positions and the in-plane relative coordinate of the exciton, respectively. We assume that the dielectric constant $\epsilon = 9.5\epsilon_0$ is the same in the ZB and WZ layers of the structure [17]. $m_e = 0.2m_0$ [18] and m_h are the electron and hole effective masses along z , respectively (we take hole effective masses of $1.76m_0$ and $1.812m_0$ in the WZ and ZB phases, respectively [18]), while μ_{\perp} is the exciton in-plane reduced mass. V_e and V_h are the conduction and valence potentials along z . The bandgaps of strain-free WZ and ZB GaN are 3.504 and 3.304 eV, respectively [19,20], while the conduction and valence band discontinuities are 270 and -70 meV, respectively [21]. We choose the following two-dimensional trial wavefunction for the exciton:

$\Phi_{\text{ex}} = f_e(z_e) f_h(z_h) e^{-\rho/\lambda} \sqrt{2/(\pi\lambda^2)}$, a choice that is justified by the ultra-thin and therefore quasi-2D character of the quantum well. $f_e(z_e)$ and $f_h(z_h)$ are the on-axis electron and hole envelope functions, respectively, and the variational parameter λ is the in-plane Bohr radius

of the exciton. To account for excitonic effects, we have used the effective potential method [22]. This method consists of injecting the chosen Φ_{ex} in Eq.(1), then averaging over the ρ and z_e dependent parts of Φ_{ex} . One then obtains a one-dimensional second order differential equation for f_h :

$$\left\{ -\frac{\hbar^2}{2} \frac{\partial}{\partial z_h} \left[\frac{1}{m_h} \frac{\partial}{\partial z_h} \right] + \tilde{V}(z_h) \right\} f_h(z_h) = E_{ex} f_h(z_h) \quad \text{Eq. (2).}$$

where $\tilde{V}(z_h)$ is an effective potential that accounts for the crystalline and Coulomb potentials felt by the hole, for the kinetic energy of the relative motion of the exciton and for the electron confinement energy [22]. One then minimizes E_{ex} against λ , obtains f_h and applies the same method to get f_e , this procedure being repeated self-consistently until full convergence of E_{ex} is achieved. In addition to E_{ex} and to the exciton binding energy E_B , we can extract the integral overlap $J = \left| \int f_e(z) f_h(z) dz \right|^2$ from our calculations. This gives access to the exciton oscillator strength per unit area $f_{ex} = 4 p_{cv}^2 J / (M E_{ex} \pi \lambda^2)$, where $M = m_e + m_h$ and p_{cv} is the momentum matrix element between the conduction and the valence bands.

It is important to account for the discontinuities of the internal polarization fields between the WZ and the ZB regions of the QW in our modeling. These discontinuities indeed give rise to charge accumulation at the WZ/ZB interfaces, causing a shift of the exciton energy via the quantum-confined Stark effect. Even in the absence of strain, crystals with WZ structure show a spontaneous polarization P_{WZ} along [0001], which is of the order of -0.029 C/m^2 [23]. Although the ZB and WZ phases exhibit a slight lattice mismatch, we neglect the effect of piezoelectric polarizations: while WZ GaN nanowires are strain free [24,25], ZB inclusions in nanowires show almost the same strain state as the WZ matrix, as shown by Raman scattering studies [26]. In the case of a single ZB layer embedded between WZ barriers, the electric field in the ZB layer is $F_{ZB} = P_{WZ} / \varepsilon$, yielding a maximum built-in electric field of $\sim 3.5 \text{ MV/cm}$ for GaN. In the situation of high-density bundles of stacking fault, however, the built-in electric fields are distributed amongst the wells and the barriers. For ZB/WZ superlattices, the conservation of the electric displacement across the homostructure leads to $F_{ZB} = L_{WZ} P_{WZ} / \varepsilon (L_{WZ} + L_{ZB})$ [27], where L_{ZB} and L_{WZ} are the thicknesses of the ZB and WZ layers, respectively.

III. Results and discussion

In Figure 1(a), we show f_e and f_h for an exciton confined in a 3 monolayer thick ZB/WZ QW, which corresponds to the case of a I₁-type BSF. In the absence of any internal polarization, we compute an exciton emission energy of 3.435 eV. This result is in good agreement with the energy of *delocalized* BSF-excitons, which ranges between 3.433 and 3.437 eV, as shown by temperature-dependent PL experiments, [16,28]. Since BSFs are shallow and narrow type-II QWs, f_e and f_h exhibit a large penetration in the WZ and the ZB phases, respectively, and we find $J = 0.822$. We note that J for a BSF-exciton is quite large compared to what was computed, for instance, for type-II GaAs/AlAs single QWs, where $J < 10^{-3}$ [22]. Thus, BSF-excitons exhibit $E_B = 30.4$ meV, which is larger than the 25 meV reported for exciton A in bulk GaN [19]. Consequently, despite the type-II band alignment of BSF, excitons confined in these planar defects are nearly bi-dimensional and show (i) an increase in binding energy compared to the bulk case and (ii) a f_{ex} of 9.10^{12} cm⁻², of the order of what observed for nonpolar (Al,Ga)N/GaN QWs with type-I band alignment [29]. In practice, BSFs in thick layers of GaN as well as ZB quantum disks in GaN WZ nanowires are found in large densities. In heteroepitaxial GaN layers grown along the a or the m axis, BSFs are distributed into bundles, where local linear densities in BSFs along the c axis as high as 10^6 cm⁻¹ have been reported [30]. Regarding the spatial extension of the BSF-exciton wavefunction out of the BSF plane, coupling between adjacent BSFs in such high-density bundles has to be considered. Thus, we show in Figure 2 the emission energy and f_{ex} computed for different BSF-BSF coupling schemes, with respect to the inter-BSF distance d . First, we find that when $d > 6$ nm, no coupling occurs and the exciton exhibits both the same energy and f_{ex} as the single BSF case. For smaller d , typically comprised between 2 and 6 nm, the exciton energy ranges between 3.42 and 3.435 eV while f_{ex} shows fluctuations ranging from -30 to +7% around the value computed for isolated BSFs. These results agree qualitatively with time-resolved cathodoluminescence experiments performed on BSFs in nonpolar GaN. While isolated BSFs show an exponential decay, the emission decay from bundles of BSFs is nonexponential [31]. We therefore attribute the nonexponential emission decay observed for bundles of BSFs to the variation of d in a given bundle, and to the subsequent variation of BSF-BSF coupling schemes. Finally, when $d < 2$ nm, we compute a redshift of the exciton emission energy down to 3.4 eV, together with an decrease in f_{ex} down to a factor of 4 for the

triple BSF system. Note that in a bundle of BSFs, the thicknesses of the WZ regions are randomly distributed. However, given that no coupling occurs when $d > 6$ nm, we infer that the properties of bundles of BSFs are likely to be similar to those computed for single, double or triple BSFs.

The influence of built-in electric fields on the BSF-exciton emission energy and overlap integral is shown in Figures 3(a)-(c). First, these fields repel the electron and hole wave functions towards opposite sides of the BSF plane (Fig. 1(b)), reducing f_{ex} . Second, in a manner similar to what happens in polar (Al,Ga)N/GaN QWs [32], built-in electric fields in BSFs lead to a redshift of the emission, the latter going from 3.435 to 3.338 eV, when the electric field amplitude is increased from 0 to 3 MV/cm (Fig. 3(a)). To our knowledge, however, such a span in the emission energies of BSF excitons in GaN has not been observed experimentally, BSF-exciton recombination energy at 10 K lying typically between 3.41 and 3.42 eV [16,28]. The latter values correspond to exciton *localized* along the plane of the BSF, whereas *free* BSF excitons are extrapolated [16,28] to recombine between 3.433 and 3.437 eV, typically. Such in-plane localization has been tentatively related to the presence of neutral donors in the vicinity of the BSFs [33]. The discrepancy between the available experimental data and the result of our calculations suggests the absence of built-in electric fields in BSFs. This may first arise from the usually high free-electron density ($>10^{16}$ cm⁻³) in nominally undoped GaN [34], the residual electrons trapped in the BSFs planes screening the electric fields [35]. This is supported by recent scanning capacitance microscopy measurements on nonpolar GaN layers, which have demonstrated that prismatic stacking faults, extended defects intersecting BSFs, exhibit a free-electron concentration higher than the surrounding fault-free material [34]. A more fundamental reason may explain the nonobservation of electric fields in BSFs. The charge density at both interfaces of polar QWs indeed shows a spatial extent of ~ 2 monolayers along the confinement direction [36]. Extending this result to a 3 monolayer thick QW, which is, really, limited to one faulty plane in the sequence of crystal planes, it is clear that there is an overlap of charged planes between the two opposite interfacial regions. The latter are certainly intermixed and, in these conditions, it is an open question as to whether built-in electric fields could be established in such a narrow QW.

Thicker homoepitaxial QWs (up to 8 monolayers) are also encountered in GaN nanowires grown along [0001] [10,37]. Increasing L_{ZB} leads to a decrease in QW emission energy, which can even lie below the ZB GaN bandgap, when polarization fields are included (Fig. 3(a)).

Also, for large L_{ZB} , the spreading of the hole wave function inside the ZB phase is suppressed, leading to a decrease in both the exciton binding energy and f_{ex} (Fig. 3(b,c)). Such a gradual reduction of f_{ex} with increasing L_{ZB} has been reported recently for homoepitaxial QWs in InP nanowires [13]. Finally, as L_{ZB} increases, so do the in-plane and on-axis spatial extensions of the type-II QW exciton wavefunction: when L_{ZB} goes from 3 to 8 monolayers, λ increases from 3.9 to 5.2 nm. Obviously, this increased spatial extension of the exciton wavefunction makes it extremely sensitive to potential fluctuations in the surrounding of the QW plane. These fluctuations may arise for instance from donor atoms distributed in or in the vicinity of the QW plane [16] or from the surface in the case of nanowires [8,25]. Whatever their origin, the multiple localization configurations available for the exciton along the QW plane contribute, together with coupling between adjacent QWs, to the broadened emission spectrum exhibited by an ensemble of nanowires [10,37]. Coming to the effect of polarization discontinuities at the ZB/WZ interfaces, crystal-phase QDs emitting below the cubic GaN bandgap have been reported [10]. This qualitatively supports our previous assumption about the absence of built-in electric fields in narrow QWs.

IV. Conclusion

In conclusion, we have computed the energy, the binding energy and the oscillator strength of electron-hole pairs in crystal phase GaN QWs and, in particular, in the most elementary case of I₁-type BSFs. Excitonic effects as well as the built-in electric fields have been included. Our calculations reveal that despite their type-II band alignment, excitons bound to BSFs show an increased binding energy compared to the bulk case. We show that coupling between adjacent BSFs occurs when the distance between adjacent faults is smaller than 6 nm and we find that BSF-BSF coupling leads to either increased or decreased exciton oscillator strength when compared to the uncoupled case. When increasing the thickness of the ZB inclusions, the wave function of the exciton gets more extended in space, making it particularly sensitive to potential fluctuations in the surrounding of the QW plane. Finally, comparing the result of our calculations with available experimental results strongly suggests the absence of built-in electric fields in the BSFs. Although this may originate from screening by residual electrons due to unintentional n -doping, we propose that the absence of electric field in BSFs actually arises from the overlap between interface charge density regions.

Acknowledgments

We acknowledge financial support from the European Union Seventh Framework Programme under grant agreement n° 265073. P. C. also thanks R. T. Phillips, B. Van Hattem, A. M. Graham, M. J. Stanley and P. Brereton for fruitful discussions and careful reading of the manuscript.

References

- [1] C. M. Lieber, and Z. L. Wang, *MRS Bulletin* **32**, 99 (2007).
- [2] R. E. Algra, M. A. Verheijen, M. T. Borgström, L.-F. Feiner, G. Immink, W. J. P. van Enckevort, E. Vlieg, and E. P. A. M. Bakkers, *Nature* **456**, 369 (2008).
- [3] P. Caroff, K. A. Dick, J. Johansson, M. E. Messing, K. Deppert, and L. Samuelson, *Nature Nanotechnology* **4**, 50 (2009).
- [4] A. Konar, T. Fang, and D. Jena, *Phys. Rev. B* **82**, 193301 (2010).
- [5] M. Murayama, and T. Nakayama, *Phys. Rev. B* **49**, 4710 (1994).
- [6] H. Shtrikman, R. Popovitz-Biro, A. Kretinin, and M. Heiblum, *Nano Lett.* **9**, 215 (2009).
- [7] M. Heiss, S. Conesa-Boj, J. Ren, H.-H. Tseng, A. Gali, A. Rudolph, E. Ucceli, F. Peiro, J. R. Morante, D. Schuh, E. Reiger, E. Kaxiras, and A. Fontcuberta i Morral, *Phys. Rev. B* **83**, 045303 (2011).
- [8] *see for instance* P. Corfdir, P. Lefebvre, J. Ristić, P. Valvin, E. Calleja, A. Trampert, J.-D. Ganière, and B. Deveaud-Plédran, *J. Appl. Phys.* **105**, 013113 (2009).
- [9] *for a review, see* K. A. Bertness, N. A. Sanford, and A. V. Davydov, *IEEE J. of Selected Topics in Quantum Electronics* **17**, 847 (2011).
- [10] G. Jacopin, L. Rigutti, L. Largeau, F. Fortuna, F. Furtmayr, F. H. Julien, M. Eickhoff, and M. Tchernycheva, *J. Appl. Phys.* **110**, 064313 (2011).
- [11] L. Zhang, J.-W. Luo, A. Zunger, N. Akopian, V. Zwiller, and J.-C. Harmand *Nano Lett.*, **10**, 4055 (2010).
- [12] N. Akopian, G. Patriarche, L. Liu, J.-C. Harmand, and V. Zwiller, *Nano. Lett.* **10**, 1198 (2010).
- [13] K. Pemasiri, M. Montazeri, R. Gass, L. M. Smith, H. E. Jackson, J. Yarrison-Rice, S. Paiman, Q. Gao, H. Hoe Tan, C. Jagadish, X. Zhang, and J. Zou, *Nano Letters* **9**, 648 (2009).
- [14] J. Ristić, E. Calleja, M. A. Sánchez-García, J. M. Ulloa, J. Sánchez-Páramo, J. M. Calleja, U. Jahn, A. Trampert, and K. H. Ploog, *Phys. Rev. B* **68**, 125305 (2003).
- [15] Y. J. Sun, O. Brandt, U. Jahn, T. Y. Liu, A. Trampert, S. Cronenberg, S. Dhar, and K. H. Ploog, *J. Appl. Phys.* **92**, 5714 (2002).
- [16] P. Corfdir, P. Lefebvre, J. Levrat, A. Dussaigne, J.-D. Ganière, D. Martin, J. Ristić, T. Zhu, N. Grandjean, and B. Deveaud-Plédran, *J. Appl. Phys.* **105**, 043102 (2009).
- [17] P. Y. Yu and M. Cardona, *Fundamentals of Semiconductors*, 3rd ed. (Springer, New York, 2005).

- [18] P. Rinke, M. Winkelkemper, A. Qteish, D. Bimberg, J. Neugebauer, and M. Scheffer, *Phys. Rev. B* **77**, 075202 (2008).
- [19] K. Kornitzer, T. Ebner, K. Thonke, R. Sauer, C. Kirchner, V. Schwegler, M. Kamp, M. Leszczynski, I. Grzegory, and S. Porowski, *Phys. Rev. B* **60**, 1471 (1999).
- [20] G. Ramirez-Flores, H. Navarro-Contreras, A. Lastras-Martinez, R. C. Powell, and J. E. Greene, *Phys. Rev. B* **50**, 8433 (1994).
- [21] C. Stampfl, and C. G. Van de Walle, *Phys. Rev. B* **57**, R15051 (1998).
- [22] A. Bellabchara, P. Lefebvre, P. Christol, and H. Mathieu, *Phys. Rev. B* **50**, 11840 (1994).
- [23] F. Bernardini, V. Fiorentini, and D. Vanderbilt, *Phys. Rev. B* **56**, R10024 (1997).
- [24] J. Sanchez-Paramo, J. M. Calleja, M. A. Sanchez-Garcia, E. Calleja, and U. Jahn, *Physica E (Amsterdam)* **13**, 1070 (2002).
- [25] O. Brandt, C. Pfüller, C. Chèze, L. Geelhaar and H. Riechert, *Phys. Rev. B* **81**, 045302 (2010).
- [26] I. Zardo, S. Conesa-Boj, F. Peiro, J. R. Morante, J. Arbiol, E. Uccelli, G. Abstreiter, and A. Fontcuberta i Morral, *Phys. Rev.* **80**, 245324 (2009).
- [27] M. Leroux, N. Grandjean, J. Massies, B. Gil, P. Lefebvre, and P. Bigenwald, *Phys. Rev. B* **60**, 1496 (1999).
- [28] P. P. Paskov, R. Schifano, B. Monemar, T. Paskova, S. Figge, and D. Hommel, *J. Appl. Phys.* **98**, 093519 (2005).
- [29] P. Corfdir, J. Levrat, A. Dussaigne, P. Lefebvre, H. Teisseyre, I. Grzegory, T. Suski, J.-D. Ganière, N. Grandjean, and B. Deveaud-Plédran, *Phys. Rev. B* **83**, 245326 (2011).
- [30] T. Gühne, Z. Bougrioua, P. Venneguès, M. Leroux, and M. Albrecht, *J. Appl. Phys.* **101**, 113101 (2007).
- [31] P. Corfdir, J. Ristić, P. Lefebvre, T. Zhu, D. Martin, A. Dussaigne, J. D. Ganière, N. Grandjean, and B. Deveaud-Plédran, *Appl. Phys. Lett.* **94**, 201115 (2009).
- [32] N. Grandjean, B. Damilano, S. Dalmaso, M. Leroux, M. Laügt, and J. Massies, *J. Appl. Phys.* **86**, 3714 (1999).
- [33] P. Corfdir, P. Lefebvre, J. Ristić, J.-D. Ganière, and B. Deveaud-Plédran, *Phys. Rev. B* **80**, 153309 (2009).
- [34] T. Zhu, C. F. Johnston, M. Häberlen, M. J. Kappers, and R. Oliver, *J. Appl. Phys.* **107**, 023503 (2010).
- [35] T. J. Badcock, M. J. Kappers, M. A. Moram, P. Dawson, and C. J. Humphreys, *Phys. Stat. Sol. (b)* **249**, 498 (2011).
- [36] *see Fig. 1 in* F. Bernardini, and V. Fiorentini, *Phys. Rev. B* **57**, R9427 (1998).

[37] H. Y. Xu, Z. Liu, Y. Y. Rao, X. T. Zhang, and S. K. Hark, *Appl. Phys. Lett.* **95**, 133108 (2009).

Figure captions

Figure 1 (color online): Band alignment (blue) and electron (red) and hole (green) envelope-functions for an exciton confined in a I_1 -BSF in GaN with zero electric field (a) and with an electric field of 1500 kV / cm (b). The effective-potential experienced by the hole (*electron*) in (a) (b) under Coulomb attraction by the electron (*hole*) is shown by the curvature of the valence (*conduction*) band profile.

Figure 2 (color online): Emission energy (symbols) and oscillator strength (line) for excitons confined in a bundle of stacking faults made of two (black) or three (red) BSFs. Dashed and dotted lines show the emission energy and the electron-hole overlap for the single-BSF case, respectively. Inset: Band alignment (blue) and electron (red) and hole (green) envelope functions for an exciton confined in two adjacent I_1 -BSFs separated by 10 monolayers.

Figure 3 (color online): Emission energy (a), binding energy (b) and overlap between electron and hole envelope functions (c) for an exciton confined in a GaN ZB/WZ homoepitaxial quantum well, with respect to the thickness of the ZB inclusion. The thicknesses of the WZ barriers have been set to 25 nm. Black squares, red dots, blue triangles, green diamonds, open purple squares and open cyan triangles correspond to built-in electric fields of 0, 100, 500, 1000, 2000 and 3000 kV / cm, respectively. In (a,b,c), the dotted lines correspond to the thickness of an I_1 -BSF.

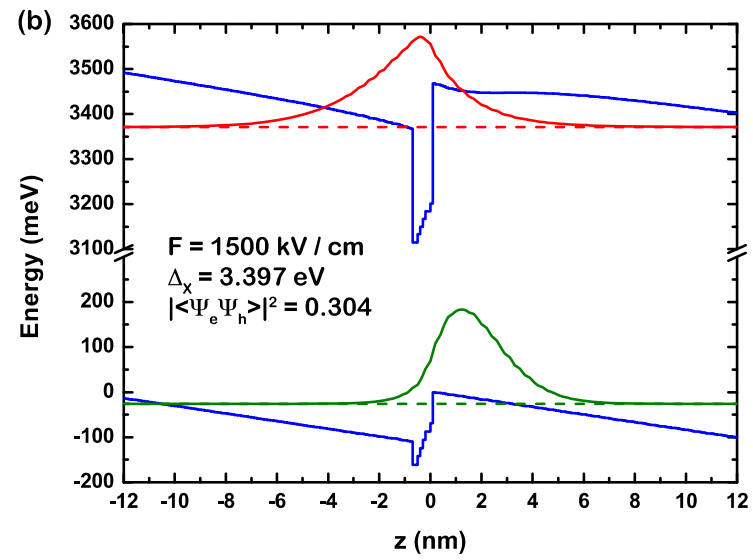
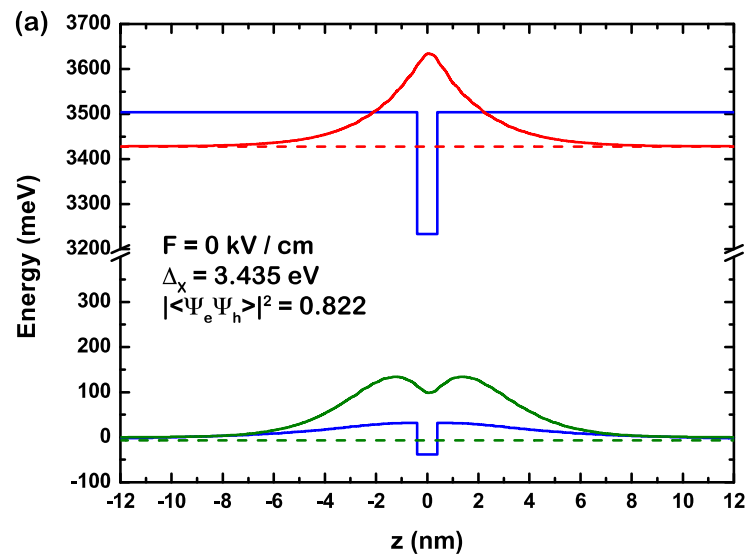


Figure 1 - Corfdir *et al.*

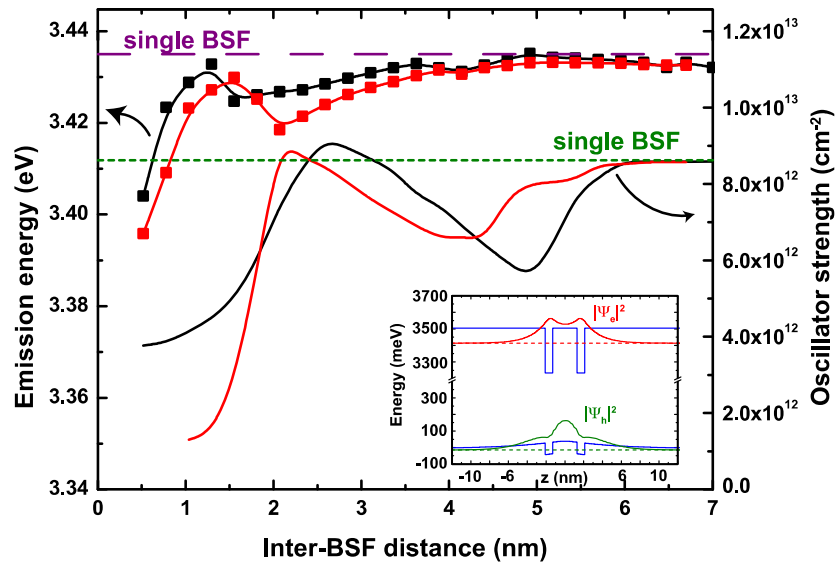


Figure 2 - Corfdir *et al.*

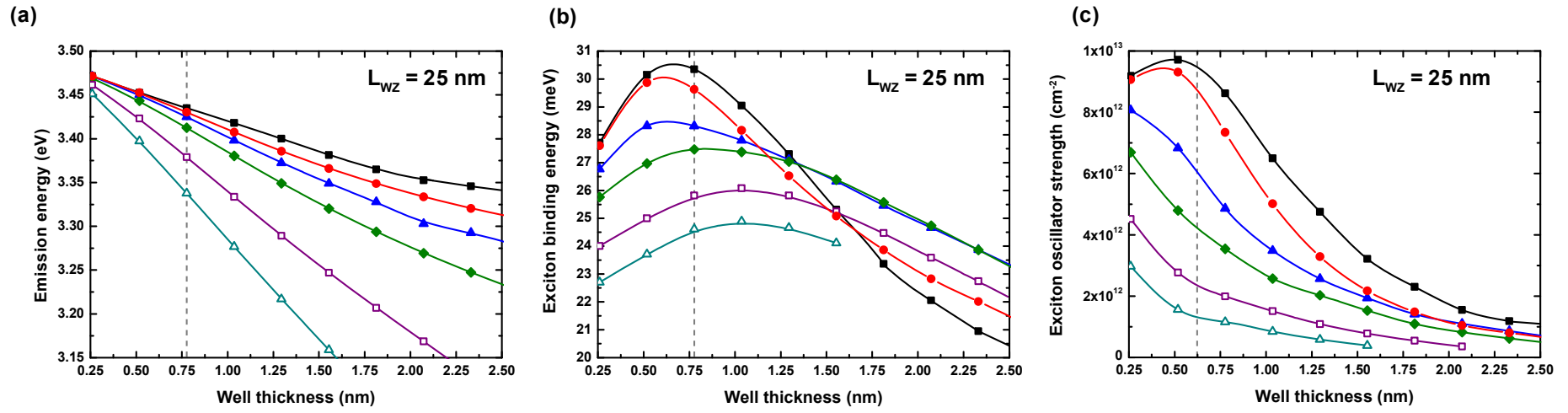


Figure 3 - Corfdir *et al.*